Laser-supported solid-state absorption fronts in silica

C. W. Carr, J. D. Bude, and P. DeMange

Lawrence Livermore National Laboratory, 7000 East Avenue, Livermore, California 94550, USA

We develop a model based on simulation and extensive experimentation that explains the behavior of solid-state laser-supported absorption fronts generated in fused silica during high intensity (up to 5 GW/cm^2) laser exposure. Both experiments and simulations show that the absorption front velocity is constant in time and is nearly linear in laser intensity. Further, this model can explain the dependence of laser damage site size on these parameters. We show that these absorption fronts naturally result from the combination of high-temperature-activated deep subband-gap optical absorptivity, free-electron transport, and thermal diffusion in defect-free silica for temperatures up to 15 000 K and pressures <10 GPa. The regime of parameter space critical to this problem spans and extends that measured by other means. It serves as a platform for understanding general laser-matter interactions in dielectrics under a variety of conditions.

I. INTRODUCTION

Laser-induced damage has important practical applications in fields from telecommunications to inertial confinement fusion.[1–4] Although much work has been done to characterize optical damage as a function of parameters such as laser pulse shape, and photon energy (E_ν), how these parameters affect the size and growth of damage sites generated during laser exposure is still not well understood.[5–9] This work helps explain the mechanisms of laser-induced damage by modeling the basic material response of silica in a regime governed by the physics of laser-matter interactions under extreme conditions.

Laser damage is a complex event governed by a variety of physical processes from energy deposition (initiation) to material ejection and fracture.[5–9] Damage sites initiate on high-quality fused silica surfaces when an absorbing defect (precursor), approximately 200 nm in diameter,[9,10] reaches high enough temperature (T) to cause mechanical damage.[11–13] Damage sites consist of a molten core surrounded by densified material and fracture[10] (e.g., see Fig. 9 Table I). Blackbody emission during laser damage shows that the cores are spatially correlated with temperatures as high as 12 000 K.[12] Furthermore, both side view scanning electron microscopy (SEM) (Ref. 7) and interferometric depth measurements suggest that a core's depth is roughly equal to its radius. Recently, it was shown that for laser intensities, I_L, less than ~10 GW/cm^2, the diameter of initiated sites scaled linearly with pulse duration (τ), for fluences, $\phi = \tau \times I_L$ up to 20 J/cm^2 and for pulse durations as low as 200 ps.[7] This indicates that the volume of absorbing material is increasing during the pulse; an absorber (precursor) with a fixed volume would absorb a total energy proportional to the pulse length (under constant intensity), and hence the final volume of heated material (after thermal diffusion) and the core diameter should scale sublinearly with pulse length.

In this work, we reproduce and extend this work under more precisely controlled conditions and explain this intriguing behavior by showing how high precursor temperature triggers additional absorption and enhanced thermal diffusion in the bulk silica. First, we develop a one-dimensional

(1D) computational model which shows how temperature-activated absorption and temperature-activated thermal diffusion naturally lead to the formation of an absorption front (AF). Next, we perform preliminary three-dimensional (3D) hydrodynamic (HD) simulations [axial-symmetric two-dimensional (2D) calculations] which include the salient physics of the 1D model to help relate 1D results to measurement. Then, we describe shaped-pulse laser damage experiments which measure how core size evolves after damage initiation as a function of laser intensity and pulse length. Both simulations and experiments show that after damage initiates, energy is deposited in a laser-supported absorption front which grows with pulse length away from the initial site of precursor absorption—longer pulses feed increasing energy deposition and result in larger cores.

II. TEMPERATURE-ACTIVATED ABSORPTION MODEL

Our premise that temperature-activated bulk absorption plays an important role in the damage process is supported by two independent observations. Laser-induced surface damage has been generated in silica without extrinsic absorbers for fluences far below the bulk material damage threshold when the surface is heated to a temperature of ~2200 K.[13] This indicates that the absorptivity of defect-free intrinsic silica, $\alpha_{INT}(T)$, increases strongly with temperature and is high enough at 2200 K to generate thermal run

TABLE I. Growth feet used to generate the sites in Figs. 9(a)–9(f) with the resultant velocity of the growth front.

Figure	I_G (GW/cm^2)	τ_G (ns)	V_F (μm/ns)
9(a)	0		
9(b)	0.25	5	0.07
9(c)	0.25	20	0.07
9(d)	0.5	5	0.19
9(e)	1.0	5	0.37
9(f)	2.0	5	0.73

away under pulsed laser illumination. In other words, once the bulk silica reaches 2200 K enhanced absorption of laser light further increases $\alpha_{INT}(T)$, and the process continues leading to destructively high temperatures. These findings are also consistent with earlier work by Papernov which suggests energy deposited at absorbing nanoparticles embedded in silica also produces enhanced absorption in the bulk silica when temperatures become high.[14]

Consequently, we explore the effect of temperature-activated absorption during a damage event using Eq. (1) which includes energy deposition, heat flow, and simple photon transport (not full radiation transport) in 1D. Here, $\kappa_{PH}(T)$ is the silica phonon thermal conductivity, $C_p(T)$ is the heat capacity, and ρ is density [values for T up to $\sim$2000 K (Ref. [15])]; t is time during the laser pulse, and x is position below the surface.

$$[C_p(T)\rho]\frac{\partial T}{\partial t} = \nabla \cdot [\kappa_{PH}(T) \nabla T] + G_{FE}(x) + I_L \alpha_{INT}(T)$$

$$\frac{\partial I_L}{\partial x} = -I_L \alpha_{INT}(T). \tag{1}$$

As previously noted, we assume initiation has just occurred at $t=0$ at a 200 nm precursor, so we employ the initial boundary condition $T(x, t=0)=8000$ K for $x<200$ nm. $C_p(T)$ is modeled[16] for $T>8000$ K. I_L is the laser intensity (constant in t) which propagates through the bulk toward the surface. G_{FE} represents a free-electron (FE) contribution to thermal diffusion and is defined below. Under these conditions, radiative and evaporative cooling were found to have little effect on energy deposition. As we are modeling the evolution of the absorbing volume, the initial size of the precursor is not critical; however, the assumption of a 200 nm precursor is based both on past work[9] and on the minimum size of damage sites observed with very short (140 ps) pulses.[10]

A variety of mechanisms can lead to increased subgap optical absorption at higher temperatures. For example, when the lattice temperature becomes high enough for significant ionic diffusion, subband-gap defect states will form which can absorb.[17] At even higher temperatures (10 000 K) and very high pressures ($>$70 GPa), a "bonded liquid" state can form which can lead to free-electron absorption.[16] Because these effects are difficult to quantify, we adopt a model for temperature-activated absorption based on Urbach broadening and band-gap narrowing which has been verified experimentally at lower temperatures. This effect is well known in semiconductors and insulators and, as it does not include ionic diffusion, serves as a lower bound for the optical absorptivity. As the temperature of a dielectric increases, phonon vibrations generate transient structural disorder and form localized electronic states in the gap (an exponentially decaying Urbach tail). The tail states are separated from continuum free-electron states by the "optical gap" E_O which shrinks with increasing temperature (band gap, E_G narrowing). For absorption of a photon of energy E_ν, this behavior is often modeled[18] as
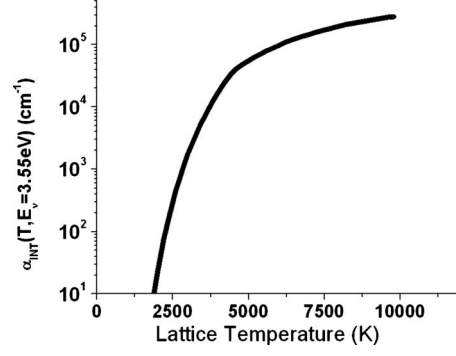

FIG. 1. Modeled optical absorptivity, $\alpha_{INT}(T)$, for photon absorption at 3.55 eV.

$$\alpha_{INT}(E_\nu) \propto \exp(E_\nu/E_U) \quad E_\nu < E_O$$

$$\propto (E_\nu - E_O)^2/E_\nu \quad E_\nu \geq E_O \tag{2}$$

where $E_O(T)=E_G-AT$, $E_U(T)=B+CT$, $E_G\sim9$ eV is the low-temperature band gap, and A, B, and C are constants. This behavior has been verified for $E_\nu>6.5$ eV and $T<1900$ K. We assume it can be extended to higher temperature and lower $E_\nu=3.55$ eV, and that E_O and E_U continue to behave linearly with respect to temperature with $A=10^{-3}$ eV/K and $B=0.02$ eV. This assumption has been justified for photon energy as low as 3.5 eV and for temperatures up to 2400 K by finite-temperature density-functional theory simulations using a hybrid functional to correct for the band gap (submitted to PRL by B. Sadigh *et al.*) We also normalize α_{INT} to be consistent with Ref. [18], under the conditions measured there. We fit C so that α_{INT}(2200 K) is large enough to support thermal runaway under the conditions of Ref. [13], and find $C=1.8\times10^{-4}$ eV/K, close to $C=1.4\times10^{-4}$.[18] Figure [1] shows the resulting $\alpha_{INT}(T)$ with $E_\nu=3.55$ eV. Here, $\alpha_{INT}(T)$ is strongly T activated: silica is essentially transparent to 3.55 eV light at room temperature, starts to absorb above 2000 K, and becomes strongly absorptive above 5000 K.

As E_O shrinks with temperature, free electron states are thermally populated. To be consistent with $\alpha_{INT}(T)$, the conduction and valence bands, E_C and E_V, follow the optical gap: $E_C-E_V=E_O$. We assume the Fermi level, $E_F=0$, is in the middle of the optical gap in order to ensure charge neutrality so that $E_C(T)-E_F=E_0(T)/2$. The free-electron density of states, the wave-vector (k) dependent velocity, $v(k)$, and free-electron energy relative to the band edge, $E(k)$, are computed using a simple effective-mass approximation fit to the silica band structure.[19] This model predicts that free-electron densities increase dramatically between 5000 and 10 000 K (Fig. [2]) in accord with optical reflectivity measurements from shocks in silica which indicate an exponential increase in FE density for temperatures in this range but for higher pressures (70–1000 GPa).[16] Thus, this model connects the band-gap narrowing regime of Ref. [18] to the bonded liquid regime of Ref. [16]. Free electrons can increase α_{INT} a few percent for $T<5000$ K but, when the gap collapses, all carriers are free; the expression here contains that transition
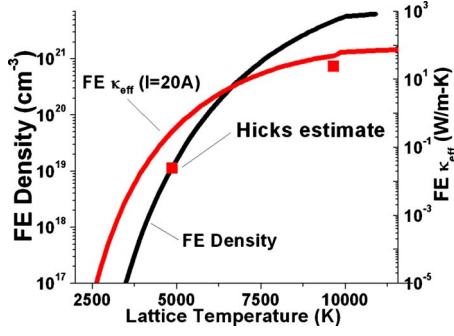
FIG. 2. (Color online) FE density and FE TC (effective thermal conductivity), κ_{eff} compared to the values observed in Ref. 16.

from direct band-to-band absorption to free-electron absorption.

In this model, free electrons cannot freely diffuse from hot to cold regions due to a large increase in $E_C(T)$ from high to low temperature—the band edge presents a band-edge energy barrier equivalent to a strong opposing electrical field.[20] However, these free electrons do add to the thermal transport. Proper treatment of free-electron heat flow requires the Boltzmann transport equation. However, in order to understand how free-electron heat conduction can affect the solution of Eq. (1), we adopt the following approach which reduces to a differential equation. Here, we assume that free electrons give up their energy within an energy loss distance l, and set the grid spacing$=l$, so that free electrons are in thermal equilibrium with the lattice at each grid point (Fig. 3). All quantities are piecewise constant at a grid point. The energy current, $J_{\text{FE}}(x_1:x_2)$, from $x_1=x-l$ to $x_2=x$ can then be expressed as Eq. (3) where $v_x(k)$ is velocity in the x direction and Θ is the Heaviside function. In this example, electrons are injected from a higher temperature point, x_1, to a lower temperature point x_2. They lose energy due to phonon scattering at x_2 (heat transfer) before diffusing back to x_1. This ensures charge neutrality, effectively reducing the net carrier current to zero while preserving a net energy transfer. The net energy transfer into a point x due to free electrons injected from $x-l$ and $x+l$ (one energy loss mean free path away) can be approximated as $G_{\text{FE}}(x)$ in Eq. (3). While the band structure and scattering cross sections are not well known at high temperatures, simulations of electron transport from Ref. 19 yield estimates of $l=1-5$ nm. Despite this uncertainty in the precise value of l, we will show below that the results under the conditions here are only weakly dependent on reasonable values of l. In the limit of small $\partial T/\partial x$, this approach reduces to classical thermal diffusion with ef-
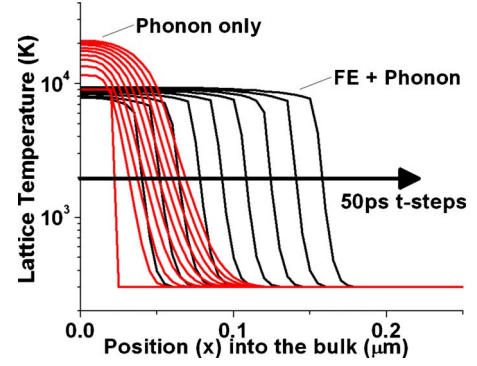
FIG. 4. (Color online) Time evolution of the AF [$T(x)$ shown in 50 ps intervals] with phonon diffusion only and with FE and phonon thermal diffusion.

fective FE diffusivity κ_{eff} [Fig. 2]: $G_{\text{FE}}(x) \rightarrow \kappa_{\text{eff}}(T)\partial^2 T/\partial x^2$. $\kappa_{\text{eff}}(T)$ is clearly temperature activated and compares well with that inferred from Ref. 16. Hence, temperature-activated absorption leads naturally to temperature-activated free-electron thermal diffusion.

$$J_{\text{FE}}(x_1:x_2) = \frac{2}{(2\pi)^3}\int_0^\infty d^3k$$

$$\times \frac{v_x(k)[E(k)-E_C(x_2)]\Theta[E(k)-E_C(x_2)]\Theta[v_x(k)]}{\exp\{[E(k)+E_C(x_1)]/k_BT(x_1)\}+1},$$

$$G_{\text{FE}}(x) = [J(x-l:x)-J(x:x-l)+J(x+l:x)-J(x:x+l)]/l. \tag{3}$$

Simulations were performed for the geometry of a beam much larger than the absorber (using a finite element explicit method with error control) for two cases: with only phonon diffusion ($G_{\text{FE}}=0$) and with both phonon and FE thermal diffusion. Figure 4 shows results for $I_L=1$ GW/cm^2. The 8000 K surface layer (precursor) activates $\alpha_{\text{INT}}(T,x=0)$ leading to high-energy deposition. As the surface layer gets hotter, heat diffusion begins to activate $\alpha_{\text{INT}}(T,x=\delta)$ at points just next to the layer. $T(x=\delta)$ increases beyond 8000 K and pushes energy deposition back further. This process continues while the laser is on creating a laser-supported solid-state absorption fronts. These absorption fronts are qualitatively similar to laser-supported combustion waves in gases,[21] and the solid-state propagating fiber-fuse effect in silica fibers.[22]

The position of the absorption front, X_{4000}, defined as the depth where $T>4000$ K ($\gg$boiling point) for $x\leq X_{4000}$, moves linearly with time resulting in a constant absorption front velocity, $V_F=dX_{4000}/dt$ as shown in Fig. 5. Other isotherms above 4000 K have indistinguishable behavior. Because nearly all of the laser energy is absorbed by the AF, the maximum absorption front temperature ($T_{\max}$) and V_F are related: $I_L \propto T_{\max}V_F$. Although phonon diffusion alone drives a front, it moves much more slowly than when free electron diffusion is included. In fact, $V_F \propto I_L^{0.5}$ with only phonons, whereas with free electron diffusion, $V_F \propto I_L^{0.8}$ (see the log-log plot in Fig. 11). When the free electron component becomes large ($T>8000$ K), energy rapidly diffuses into the adjacent
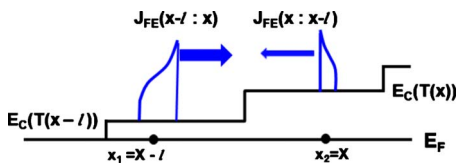

FIG. 3. (Color online) Flow of heat due to FE diffusion across the energy barrier between grid points $x-l$ and x with $E_F=0$. FE energy distributions and energy current shown in blue; energy shown vertically.
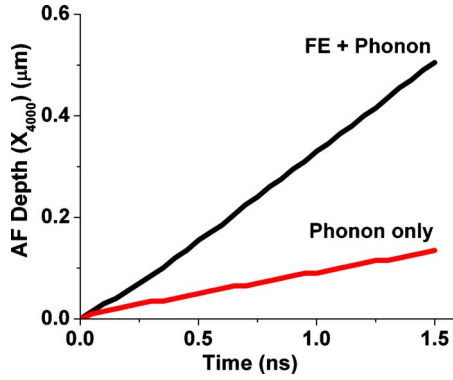
FIG. 5. (Color online) The depth of the 4000 K isotherm as a function of time for both the phonon only and the FE+phonon models.

cool region, pinning T_{max} near 10 000 K—close to the black-body measurements of Ref. 12. High free-electron thermal conductivity also distributes energy absorbed at the front throughout the expanding heated zone. Because T_{max} can then only increase weakly with I_L, and $I_L \propto T_{max} V_F$, V_F becomes nearly linear in I_L. Without FE contributions, both T_{max} and V_F increase, and T_{max} can then become much larger ($>$40 000 K) than measured values.[12] When the pulse (and energy deposition) ends, there is very little further thermal diffusion, and $V_F \rightarrow 0$; hence, the absorption front is laser supported.

In order to relate the physics of 1D absorption fronts to measured damage sites, we included temperature-activated absorption and free-electron thermal diffusivity in 2D axial symmetric (R=radial, x=axial, or depth direction) HD simulations which were solved using Arbitrary Lagrange/Eulerian in 3D (ALE3D).[23] ALE3D uses a Thomas-Fermi-based equation of state model described by Young and Corey.[24] As in the 1D model, we use the HD simulations only to assess the evolution of energy deposition while the laser is on and to investigate the formation and evolution of an AF. The HD simulations have been performed in particular to understand the role of 3D transport and material motion but are not meant to be comprehensive. A more sophisticated treatment is required to model material ejection and mechanical processes such as fracture which occur after the laser pulse; this treatment is beyond the scope of this work. Since we are modeling exit surface damage, the laser reaches the AF below the surface from the back side, and energy deposition is not affected by these more complex processes as it would be in the case of laser ablation where the laser pulse strikes the surface from the front (air) side where the laser would be intercepted by the ejecta plume.

The HD simulations here include photon transport, and $\alpha_{INT}(T)$ and k_{PH} as in Eq. (1) but approximate G_{FE} with a $k_{eff}(T)$ similar to that defined above. To mimic the 1D case, the initial condition was a 8000 K, 100 nm hemisphere at the surface (x=0); I_L propagated in x through the bulk toward x=0. Simulations were performed up to 2 ns for I_L =1.2 GW/cm^2. As in the 1D case, we found that an absorption front formed while the laser was on, and that it propagated with linear V_F away from the initial heated region; furthermore, the absorption front expanded in all directions.
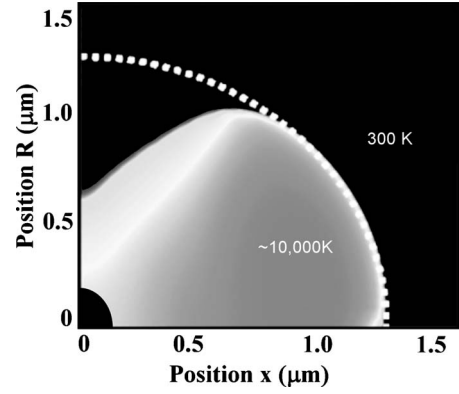

FIG. 6. Temperature profile from HD simulation with 2 GW/cm^2, after 2 ns; the initial state is the black dot at R=x=0; expected core region outlined.

Figure 6 shows the simulated temperature profile after 2 ns with I_L=2 GW/cm^2. The size of the absorption front is defined by the maximum extent of the region $>$4000 K in the R and x directions. Radial and axial absorption front velocities, V_{FR} and V_{FX} were 0.75 μs/ns and 1.05 μm/ns, respectively. The primary HD effect was thermal expansion which increased V_F somewhat compared to the 1D case [see Fig. 11] but V_{FX} is clearly consistent with 1D results; peak P $<$ 10 GPa, and shock heating did not affect energy deposition. The primary 3D effect was shadowing of I_L at the surface by absorption from the AF expanding in the radial direction below it. This causes the absorption front to grow broader as it evolves deeper. Shadowing is sensitive to the details of light propagation toward the AF. We estimate that lensing due to density gradients beneath the absorption front slightly focuses I_L, reducing shadowing and asymmetry. Though HD calculations representing the lensing effects by using focusing light recovered the hemispherical geometry, more comprehensive 3D HD simulations can help clarify these effects.

These preliminary HD simulations confirm the key results of the 1D treatment. They show that a high temperature (near 10 000 K) region forms at the surface which expands linearly in x and R. An expanding absorption front intercepts a larger cross section of laser energy as a function of time; this is why the core volume grows linearly with τ, not with fluence absorbed in a fixed point source as noted in Sec. I. As per the simulations, the material within the AF is heated to temperatures near 10 000 K, well beyond the melting point of the material and within a regime where the evaporation rate is very high (the vapor pressure of silica is 1 atm at about 3000 K). A material heated to these temperatures in a few nanoseconds is likely to be superheated and will be ejected from the surface by explosive boiling or fast evaporation leaving a molten core. This is supported by the SEM images of damage site cores in Fig. 9 which show molten ejecta fibers. These damage site cores should be roughly the size of the maximum extent of the absorption front as outlined in Fig. 6. The core radius tracks the absorption front depth, indicating that the damage site core should grow linearly with time. Indeed, side view SEM measurements[7] as seen in Fig. 7 indicate that the depth to radius ratio of the
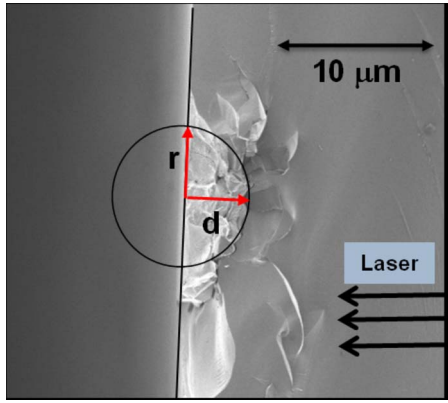
FIG. 7. (Color online) A side-view SEM obtained by cleaving though a damage site. The damage site was on the exit surface of the optic as noted by the direction of the laser. The area in the SEM was entirely and evenly illuminated by the laser.

damage site cores is approximately 1:1. Hence, measured core radii give a good estimate of core depth. Furthermore, 1D simulations provide reasonable estimates for core depth. This allows us to compare the behavior of the 1D absorption front velocities ($\sim V_F$ in the depth direction) with measured trends in rate of increase in the core radius versus laser intensity.

III. EXPERIMENT

Two-inch diameter, polished fused silica windows (CVI-Melles Groit) were cleaned with detergent and an ultrasonic DI water rinse. Regions of the samples were exposed by the Optical Science Laser facility to single laser pulses with various temporal pulse shapes (see Fig. 8).[25] The laser pulse passed through the bulk to initiate damage on the exit surface. The diameter of the laser beam (1 cm) is very large
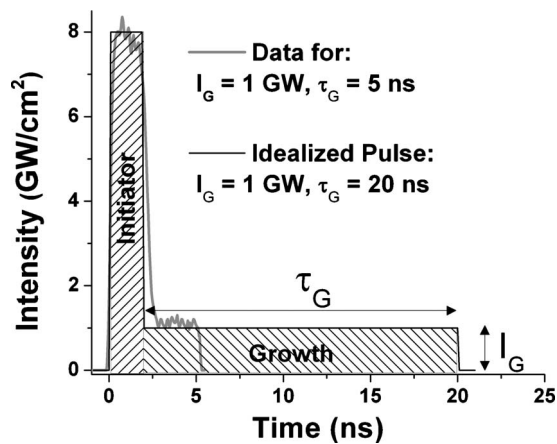

FIG. 8. The pulse shape used to produce damage consisted of an initial 2-ns-long 8 GW/cm^2 initiator section which set a constant initial state for the absorption front. The AF initiator was followed immediately by one of various growth "feet" defined by their intensity I_G and duration τ_G. The two sections of the idealized pulse are shown in hash. The measured pulse shape for an initiator pulse with a 2.5 ns 1 GW growth foot is shown in gray.
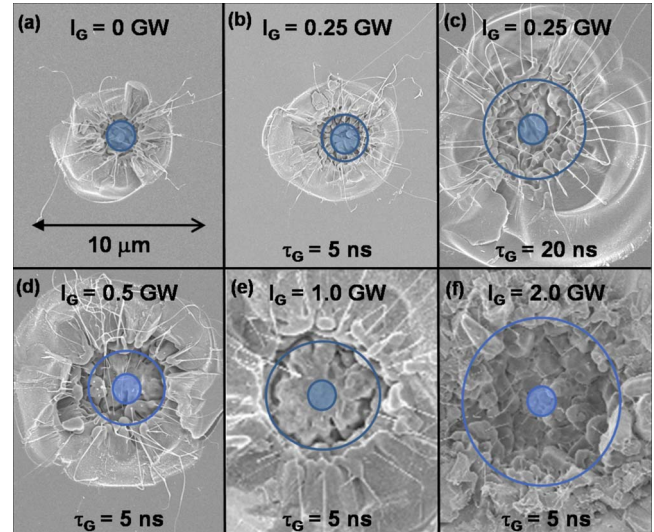

FIG. 9. (Color online) Damage sites produced by AF initiator pulses followed by various growth feet. The size bar is common to all six images. The core is identified as the molten region in the SEM images which show the evidence of explosive ejection. The values of I_G, τ_G, and calculated velocities for images (a)–(f) can be found in Table I. In each image, the solid blue circle indicates the average measured diameter of cores created with the AF initiator pulse without a growth foot. The outer blue circle indicates the average measured D of the core under different growth pulse conditions. SEM images were chosen to match the average values of the sties created under those conditions.

compared to the size of the damage sites (see below). Because damage is initiated on the exit surface, vaporized and ejected material does not interfere with the interaction of the laser with the bulk silica. These experimental conditions are well represented by the calculations described above.

The pulse shapes used can be categorized in two classes, the first of which was the absorption front initiator pulse—$\lambda = 351$ nm (3.55 eV), with a pulse length $\tau = 2$ ns, and an intensity $I_0 = 8$ GW/cm^2— used to establish a constant initial state of the absorption front. The second class of pulse was the probe pulse, which consisted of an absorption front initiator pulse followed immediately by a constant intensity foot intended to grow the absorption front under conditions of controlled intensity and duration. The intensity and duration of the foot were varied from pulse to pulse up to ≤ 6 GW/cm^2 and ≤ 20 ns, respectively. These conditions initiated about ~ 10 damage sites/mm^2 for all pulse shapes except for cases when the foot exceeded 4 GW/cm^2, which initiated additional sites. SEM images were taken of 10–50 isolated surface sites (Fig. 9) created by each pulse shape. As reported previously,[10] an easily identifiable molten core (herein, D is the core diameter) with ejecta fibers was found in most sites. The average D of 16 sites created by the absorption front initiator pulse was 2.1 ± 0.35 μm and is indicated by the solid blue circle in Fig. 9(a). Similar treatment was used for extracting diameters measurements for all other pulse shapes which did not produce additional damage during the growth foot. For the two cases where the density of sites was increased by the growth foot ($I = 4$ GW/cm^2 and $I = 5$ GW/cm^2) only the largest sites were measured. This
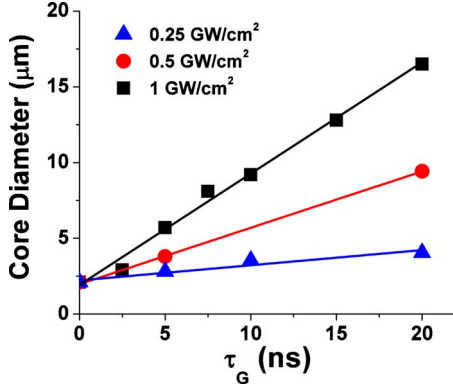
FIG. 10. (Color online) Points are the average experimentally measured core diameters, D. For each series (with $I_G = 0.25$, 0.5, and 1 GW/cm^2, respectively) D is plotted versus the duration of the constant growth intensity. The lines are linear fits with the slopes reported as velocities (V_F) in Fig. 11.

was necessary because sites created during the growth foot would not be grown by the entire foot and thus should not be ascribed to a growth foot of the full duration. For growth feet of 6 GW/cm^2 and above, the majority of damage sites were created during the growth foot precluding meaningful size measurements. For total fluences above 30–40 J/cm^2 fracture in the surrounding material began to dominate the damage site morphology.

IV. DISCUSSION

The 2 ns initiation pulse reproducibly generates initiations with a small ($D \sim 2$ μm) superheated surface zone; this is modeled as the initial 8000 K surface condition in the simulations. The core diameters [Figs. 9(a)–9(c) and 10] show a linear dependence on τ_G for constant I_G corresponding to the model results. V_F for these experiments is defined in analogy with the model; the experimental V_F is the rate of increase in radius of the core due to the foot: $V_F = (R_G - R_C)/\tau_G$, where R_G is the radius of the core generated with the growth pulse and R_C is the radius of the control core.
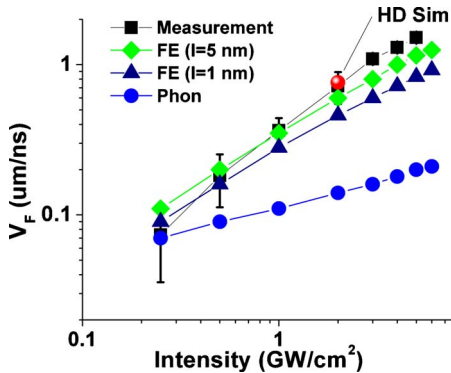

FIG. 11. (Color online) Comparison of modeled and experimental V_F with FE indicating the full FE+phonon model with $l = 1$ nm and 5 nm, respectively; Phon is the phonon only model. Simulated V_F's are all 1D except for the 2 GW/cm^2 HD point noted.

Figure 11 directly compares the measured V_F with modeled V_F (1D except for where noted) for growth I_G up to ~ 5 GW/cm^2. Measured V_F is shown along with error bars. Note, under these conditions, V_F is substantially lower than the speed of sound in silica (5.8 μm/ns), confirming simulations that the AF does not follow a shock. Instead, measured V_F is close to the modeled results. Here, simulations were performed separately using phonon thermal diffusion alone, and with the addition of the free-electron component of thermal diffusion. For the simulations including the free-electron component, values of $l = 1$ and 5 nm were used. While measurements and both models give constant V_F as a function of time, the phonon-only thermal-diffusion model underpredicts measurement by more than a factor of three at 1 GW/cm^2 and has the wrong behavior versus laser intensity, I_L; measurements are much closer to the $V_F \propto I_L^{0.8}$ behavior when free-electron thermal diffusion is added, and the numerical agreement gets much closer. The comparison in Fig. 11 shows that this model can predict the behavior of absorption front propagation in silica over a factor of 20 in laser intensity (0.25–5 GW/cm^2). The ratio of the absorption front velocity to laser intensity is likely valid beyond 5 GW/cm^2, but the occlusion of the damage site cores by extensive fracture and additional initiations in the growth section of the pulse prevented reliable measurements in this regime.

The velocity of the absorption front is not very sensitive to l; a factor of 5 change in l makes only $\sim 35\%$ change in V_F. In fact, modeled V_F is a weak function of quantities like l which are most uncertain. Scaling G_{FE} by a factor of ten around that used here only changes V_F by $\sim 30\%$. V_F is fairly insensitive to α_{INT} if it exceeds about 5×10^4 cm^{-1} for $T > 10\,000$ K. T_{max}, using the FE thermal-diffusion model, agrees well with T measured in Ref. 12: 8000 K ($I_G = 0.25$ GW/cm^2) to 13 000 K ($I_G = 5$ GW/cm^2). Damage sites with core diameters exceeding ~ 10 μm begin to lose definition because the morphology of the sites becomes dominated by deep fractures in and around the region of the damage site. This behavior may be explained by a complex material response to deep superheated material, which would require full HD treatment including fracture and self-consistent optical simulation.

V. CONCLUSION

In this work we have demonstrated that the majority of energy deposited during laser-induced damage on the exit surface of SiO$_2$ occurs during a laser-driven absorption front. For laser intensities less than 5 GW/cm^2, the velocity of the front is nearly linear in intensity. This behavior is driven principally by the T-activated deep subband-gap (3.55 eV) absorptivity, free-electron transport and thermal diffusion of silica for temperatures up to 15 000 K and pressures less than 10 GPa. Solid-state AFs will naturally result from the combination of high-temperature-activated absorptivity and thermal conductivity in any material with these properties. Any material which exhibits strong temperature-activated optical absorption should generate a laser-driven solid-state absorption front. Urbach broadening and band-gap narrow-

ing provide a plausible mechanism for temperature-activated absorption and the temperature-activated thermal conductivity linked to it, though other mechanisms may also play a role. The regime of parameter space critical to this problem spans and extends that measured by other means including direct measurements of T-activated absorption for photon energies >6.5 eV and $T<1900$ K,[18] and thermal diffusivity inferred from shock experiments for $T>5000$ K and $P>70$ GPa.[16]

While laser damage is governed by many factors, the formation of an absorption front is a key step in this process; absorption fronts are also relevant to experiments or techniques which involve laser-driven shocks through dielectrics. More broadly, this model serves as a platform for under-

standing general laser-matter interactions in dielectrics including laser-supported solid-state absorption fronts in a variety of materials under various conditions.

[1] C. W. Carr, M. D. Feit, M. C. Nostrand, and J. J. Adams, Meas. Sci. Technol. **17**, 1958 (2006).

[2] M. Ushio, K. Komurasaki, K. Kawamura, and Y. Arakawa, Shock Waves **18**, 35 (2008).

[3] S. I. Yakovlenko, Laser Phys. **16**, 1273 (2006).

[4] J. D. Lindl, P. Amendt, R. L. Berger, S. G. Glendinning, S. H. Glenzer, S. W. Haan, R. L. Kauffman, O. L. Landen, and L. J. Suter, Phys. Plasmas **11**, 339 (2004).

[5] C. W. Carr and J. M. Auerbach, Opt. Lett. **31**, 595 (2006).

[6] R. A. Negres, M. D. Feit, P. DeMange, J. D. Bude, and S. G. Demos, Proc. SPIE **6720**, 672019 (2008).

[7] C. W. Carr, M. J. Matthews, J. D. Bude, and M. L. Spaeth, Proc. SPIE **6403**, 64030K (2007).

[8] C. W. Carr, H. B. Radousky, and S. G. Demos, Phys. Rev. Lett. **91**, 127402 (2003).

[9] M. D. Feit and A. M. Rubenchick, Proc. SPIE **5273**, 74 (2004).

[10] C. W. Carr, M. D. Feit, M. A. Johnson, and A. M. Rubenchik, Appl. Phys. Lett. **89**, 131901 (2006).

[11] S. Palmier, M. A. Josse, H. Bercegol, R. Courchinoux, L. Lamaignere, J. L. Rullier, and B. Bertussi, Proc. SPIE **6720**, U576 (2008).

[12] C. W. Carr, H. B. Radousky, A. M. Rubenchik, M. D. Feit, and S. G. Demos, Phys. Rev. Lett. **92**, 087401 (2004).

[13] J. Bude, G. Guss, M. Matthews, and M. L. Spaeth, Proc. SPIE **6720**, 672009 (2008).

[14] S. Papernov and A. W. Schmid, J. Appl. Phys. **92**, 5720 (2002).

[15] S. T. Yang, M. J. Matthews, S. Elhadj, V. G. Dragoo, and S. E. Bisson, J. Appl. Phys. **106**, 103106 (2009).

[16] D. G. Hicks, T. R. Boehly, J. H. Eggert, J. E. Miller, P. M. Celliers, and G. W. Collins, Phys. Rev. Lett. **97**, 025502 (2006).

[17] J. Horbach and W. Kob, Phys. Rev. B **60**, 3169 (1999).

[18] K. Saito and A. J. Ikushima, Phys. Rev. B **62**, 8584 (2000).

[19] D. Arnold and E. Cartier, Phys. Rev. B **46**, 15102 (1992).

[20] K. Hess, *Theory of Semiconductor Devices* (IEEE Press Marketing, Piscataway, NJ, 2000).

[21] M. V. Allmen, *Laser-Beam Interactions with Materials* (Springer, Lexington, MA, 1987).

[22] D. P. Hand and P. S. Russell, Opt. Lett. **13**, 767 (1988).

[23] A. Anderson, B. Arrighi, R. Becker, T. Dunn, D. Faux, G. Friedman, B. Liu, R. McCallen, F. Najjar, R. Neely, , A. Nichols, D. Nikkel, T Pierce, J. Reus, R. Settgast, B. Wallin, D. White, and J. Yao, LLNL Report No. UCRL-SM-404490, 2009 (unpublished).

[24] D. A. Young and E. M. Corey, J. Appl. Phys. **78**, 3748 (1995).

[25] M. C. Nostrand, T. L. Weiland, R. L. Luthi, J. L. Vickers, W. D. Sell, J. A. Stanley, J. Honig, J. Auerbach, R. P. Hackel, and P. J. Wegner, Proc. SPIE **5273**, 325 (2003).